The Vanadium Redox Flow Battery - Electrochemical Impedance Characterization

Joana Dias Fonseca
joana.d.fonseca@tecnico.ulisboa.pt

Instituto Superior Técnico, Universidade de Lisboa, Portugal

January 2021

Abstract

With the increasing use of intermittent renewable energy sources, such as solar and wind energy, electricity storage systems such as redox flow batteries have been the target of growing interest. In this work, the electrochemical characterization of a Vanadium Redox Flow Cell (25 cm^2) was performed. Polarization curves were taken where current densities achieved 11 mA/cm^2 and 92 mA/cm^2 for an electrolyte with vanadium concentration of 0.125 M and 1.21 M, respectively. Electrochemical Impedance Spectroscopy (EIS) measurements were made for different experimental conditions to study the response of the cell. The ohmic resistance of the cell for standard experimental set up and a vanadium concentration of 0.125 M was found to be 3.9 Ω cm^2. The faradaic resistance varied with the State of Charge (SOC) and ranged from 3.8 to 13 Ω cm^2, its lowest value at 30-70% SOC. The charge-transfer resistance increases 15.2 times with the removal of the carbon felts, and mass transport variations were also observed. The economic assessment of a VRFB installation in a "Recheio" Supermarket in Tavira was performed and the project resulted in a positive Net Present Value (NPV) of 43 247 € after 20 years.

Keywords: Vanadium Redox Flow Battery; Electricity Storage Systems; Electrochemical Impedance Spectroscopy; Economical Evaluation

1. Introduction

Energy storage systems (ESS) have been around since the beginning of times, but more focus has been drawn to them now that renewable energy sources (RES) have become so popular and their intermittent nature requires storage systems to manage the supply and demand of electricity. Battery energy storage systems (BESS) are practical devices that can be used in both mobile and stationary applications. Lead-acid batteries have been market leaders for the last decades. The positive electrode consists of porous lead dioxide and the negative electrode is finely divided lead [14]. The great advantage of lead-acid batteries lies on their low cost of installment (206 €/kWh [12]), as well as good storage efficiency of 85% [14, 5]. These batteries can also reach 100% rates of recycling [4]. Some drawbacks include the short life-time of only 10 years [14]. Lithium-ion batteries (LIB) have become incredibly popular over the last decade. They're based on the migration of lithium ions from anode to cathode and vice-versa, while compensating electrons travel in the external circuit. The most valuable feature of lithium-ion batteries is their high energy density (up to 200 kWh/kg), which makes them highly suitable for mobile applications [3], and great efficiency of 93% [19]. However, materials are flammable and reactive. It also shows short life-time. A new technology, presenting long life-time and able to decouple energy from power, has been developing: redox flow batteries (RFB), specially All-vanadium redox flow batteries (VRFB). Electrolyte containing the diluted redox couple is stored outside the cell and gets circulated by pumps through the cell's inert electrodes, where the electroactive species are oxidized or reduced. In VRFB, active species are four oxidation states of the same element, vanadium: V^{2+}, V^{3+} at the negative half-cell and VO^{2+} and $VO_2{}^+$ at the postive half-cell. In this work, the electrochemical characterization of a VRFB cell was conducted with special emphasis on the Electrochemical Impedance Spectroscopy (EIS) technique.

2. Vanadium Redox Flow Batteries

2.1. Nernst Equation and State of Charge

The reactions taking place in a VRFB during discharge at the anode and cathode are, respectively:

$$V^{2+} \longrightarrow V^{3+} + e^- \tag{2.1}$$

$$VO_2^+ + 2\,H^+ + e^- \longrightarrow VO^{2+} + H_2O \qquad (2.2)$$

The standard reduction potential E°, that is, at 25 °C, 100 kPa and solutes at a concentration of 1 M, for the anode and cathode reactions is -0.26 V and +1.0 V, respectively, and the standard potential for the cell becomes 1.26 V.

The Nernst equation, allows us to know the equilibrium potential of an electrode for its specific conditions of temperature, pressure and concentration of solutes:

$$E_{eq} = E^\circ - \frac{RT}{nF} \ln K \qquad (2.3)$$

where n is the number of electrons transfered in the reactions, R is the gas constant, T is the temperature and K stands for the equilibrium constant. To account for activity coefficients that are difficult to measure and concentration of hydrogen ions, the formal potential $E^{0'}$ is introduced as the potential at which the cell is at 50% state of charge (SOC) and:

$$E^{\circ\prime} = E^\circ + \frac{RT}{F} \ln \frac{\gamma_{VO_2^+}\gamma_{V^{2+}}(H^+)^2}{\gamma_{V^{3+}}\gamma_{VO^{2+}}} \qquad (2.4)$$

The final equation for the equilibrium potential of the cell is:

$$E_{eq} = E^{\circ\prime} + \frac{RT}{F} \ln \frac{[VO_2^+][V^{2+}]}{[V^{3+}][VO^{2+}]} \qquad (2.5)$$

and the SOC can be computed by:

$$SOC = \frac{\exp\left(\frac{F}{2RT}(E_{eq} - E^{\circ\prime})\right)}{1 + \exp\left(\frac{F}{2RT}(E_{eq} - E^{\circ\prime})\right)} \qquad (2.6)$$

2.2. Performance Indicators

The total **capacity** of a cell stands for the total amount of charge that can be supplied to the external circuit [20]. The capacity depends on the amount of electrochemically active species available and the number of electrons being transfered for every mole of reagent converted. The theoretical capacity of the cell can be given by:

$$Q_T = xFN_M \qquad (2.7)$$

where x stands for the number of moles of electrons transfered during the conversion of one mole of reagent and N_M stands for the number of moles of limiting reagent. If the electrolytes are balanced and have the same number of moles, N_M for a VRFB can be found multiplying the concentration of vanadium inside the electrolyte by its total volume. This shows how the capacity of the VRFB is directly proportional to the volume and concentration of electrolyte, which is stored externally to the cell and can be easily scaled up [11].

In practice, the actual capacity is always different from eq:theoreticalcapacity due to different phenomena that will "consume" the reactants without contributing to the generation of current, like side reactions and crossing-over of ions. The battery's actual capacity is the number of coulombs or ampere hours delivered [20] and can be computed by:

$$Q_P = \int_0^t i\,dt \qquad (2.8)$$

where i stands for the current flow for a period of time t.

Self-discharge is a phenomenon in which capacity is lost even when the battery is not under load. In a VRFB, self-discharge considers two different conditions, as opposed to other technologies. If the electrolyte is being pumped but there is no current flowing, self discharge considers not only the typical vanadium cross-over through the membrane but also the consumption of energy through auxiliary devices such as pumps. When the cell is in standby, self-discharge accounts mainly for crossing-over, which only occurs within the cell and not inside the tanks [11].

3. Electrochemical Techniques

3.1. Polarization curves

Typical polarization curves for electrochemical cells usually show three different regions, as it can be seen in Figure 1. In the first region, for low current density, an intense voltage drop is seen, due to the activation overpotential. The second region is almost linear, consisting in ohmic losses, and it is associated with the internal resistance of the cell, which includes the ionic resistance of the electrolyte, the ionic resistance of the membrane and the mass-transfer of redox-active species within active electrode areas. The third and final region stands for the transport losses [20]. As the voltage decreases, the current is unable to keep a linear evolution, and we see it decay to a limiting current.

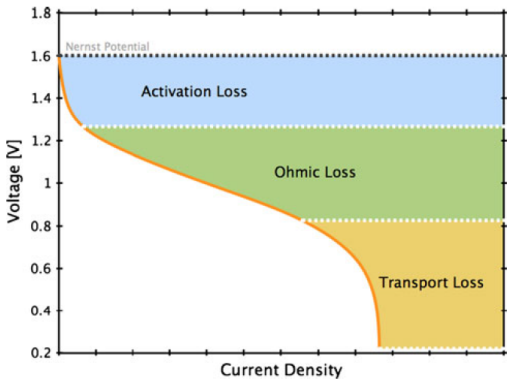

Figure 1: Generalized polarization curve for a VRB indicating the dominant source of overpotential in each region [2].

3.2. Electrochemical Impedance Spectroscopy

One of the advantages of Electrochemical Impedance Spectroscopy is that it can be performed several times without altering the electrochemical properties of the system. a small sinusoidal voltage perturbation (5 to 20 mV) of known amplitude and frequency is applied, creating a current response, also sinusoidal, and the impedance of the system is the relationship between them, taking into account both phase shift and amplitude of the signals [6, 16]. Using an expression homologous to the Ohm's Law, the impedance of the system is given by:

$$Z(\omega) = \frac{E}{I} = |Z|\cos\Phi + |Z|\sin\Phi j \qquad (3.1)$$

Electrochemical cells are usually represented by an equivalent circuit consisting of a resistor in series with two resistor-capacitor parallel networks, as seen in Figure 2. Each circuit element represents a different physical phenomenon occurring inside the cell. R_S, the series resistance, stands for the ohmic drop inside the cell and is the interception of the graph with the horizontal axis at high frequencies. Two capacitive loops then follow, represented by two resistor-capacitor parallel networks in the circuit model. The first loop is often attributed to charge-transfer effects, its diameter R_1 accounting for the charge-transfer resistance and the capacitor representing the double-layer formed at the electrodes' interface. At low frequencies the transport effects are represented.

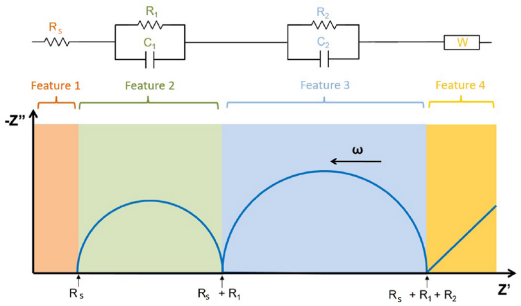

Figure 2: Schematic idealized impedance complex plane plot for a VRFB cell [1]

4. Experimental Methods

4.1. Electrolyte Preparation

Two concentrations of vanadium were used in the experiments, 1.25 M and 0.121 M, and a sulfuric acid concentration of 5 M. From a solution of vanadium pentoxide, the electrolyte was prepared adding oxalic acid to convert all VO_2^+ species to VO^{2+}, and then zinc was added to get a 50/50 mixture of VO^{2+} and V^{3+}. The mixture was fed to the cell and current was applied to have a v3+ solution at the negative half-cell and VO_2^+ at the positive one, which represents the cell at 0% and it is ready to use.

4.2. Cell Assembly

Assembly of the cell was performed as the scheme in Figure 3. The cell has 25 cm^2. As electrodes SGL Carbon Sigracell GFB 6 EA carbon felts, graphite plates were of the Sigracell PV15 and the current collectors are made of copper. Silicone gaskets were used to avoid leakage. The Dupont Nafion membrane used was first prepared following the method in [15].

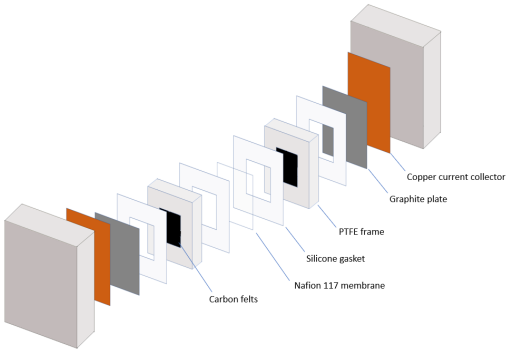

Figure 3: Schematic of the assembly of the cell.

4.3. Testing conditions

All measurements were made using a Gamry 5000 Potentiostat. The values of current density and impedance are normalized for an active area of 25 cm^2. The fittings to all the experimental data from EIS were performed using the ZView software. For

polarization curves, a scan rate of 0.002 A/s was used. EIS measurements were performed for a frequency range of 100000 Hz to 0.03 Hz, AC voltage of 5 mV at 8 points per decade.

5. Results and Interpretation

Charge/discharge curves measured with no electrolyte circulation were used to determine the formal potential from the 50% point. The computed formal potential was 1.43 V, which is slightly higher than what other authors [17, 10, 7] obtained, but different concentrations of vanadium and acid were used. This value was used to relate the open circuit potential (OCP) with the SOC of the cell through Equation 2.6.

5.1. Polarization curves

As seen in Figure 4, the limit current undergoes a 17% increase between flow rates of 9.4 to 20.4 mL/min, an evolution that is in agreement with results obtained by Aaron et al [2]. For a low vanadium concentration of 0.125 M, current density reaches its limit at 9.2 mA/cm^2. Higher concentration of electrolyte allowed to reach higher current densities of 90 mA/cm^2, as seen in Figure 5.

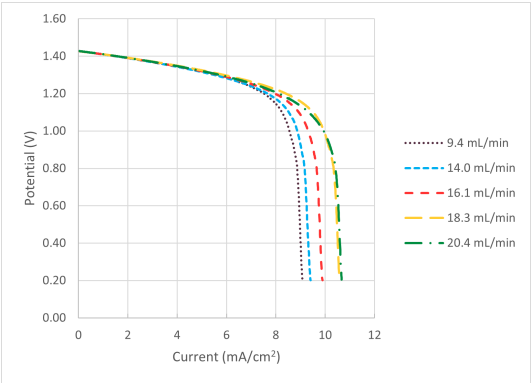

Figure 4: Discharging polarization curves for a concentration of 0.125 M at different flow rates, with a scan-rate of 2 mA/s.

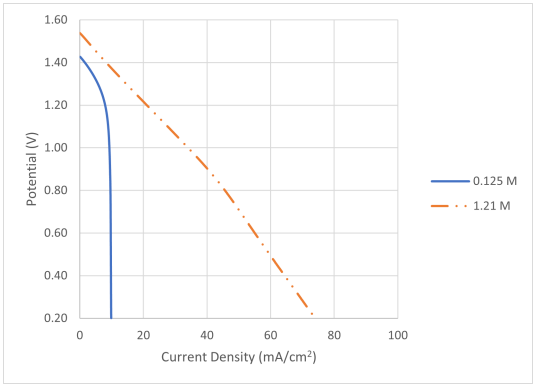

Figure 5: Polarization curves at a flow rate of 16.1 mL/min for different vanadium concentrations, 1.21 M and 0.125 M, with a scan-rate of 2 mA/s.

5.2. Electrochemical Impedance Spectroscopy

To test the effect of the number of membranes in the cell's resistance, EIS measurements were performed using 1, 2 and 3 Nafion membranes, and a significant increase in ohmic resistance is found - fig:membranes).

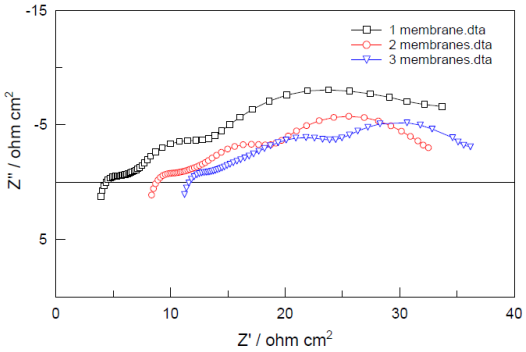

Figure 6: Impedance spectra of the VRFC with the setup using single or multiple Nafion membranes; flow rate 20.4 mL/min, vanadium concentration of 0.125 M.

From Figure 7 a direct proportionality between the ohmic resistance and the number of membranes is evident. The interception with the origin reveals that the membrane is the main component contributing to the cell's ohmic resistance, which is 3.9 Ωcm^2. The resistance of the Nafion 117 membrane is 3.8 Ωcm^2.

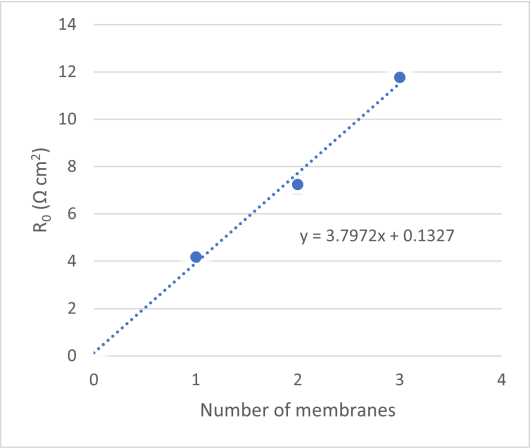

Figure 7: Fitting result directly taken from ZView Software for the Nyquist plot obtained for one membrane, where units for R are Ω cm^2, for CPE-T are F cm^{-2}s$^{\alpha-1}$, and CPE-P has no units.

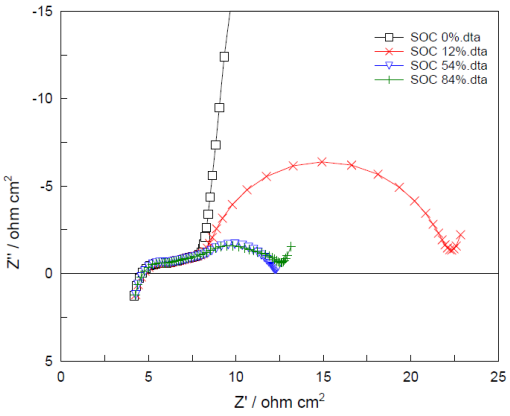

Figure 9: Impedance spectra of the VRFC obtained for different levels of SOC; vanadium concentration of 0.125 M and stagnant electrolyte.

In Figures 8 and 9 the EIS spectra for different SOC are presented with and without electrolyte circulation. The same tendency is observed for both conditions and the faradaic resistance is affected by the SOC, as it can be seen in Figure 10. R_2 ranges from 3.8 to 13 Ω cm^2. The reaction rate is maximum at SOC in a medium range, 30-70%, while the reaction seems to be slower at very high or very low SOC, which was previously seen by other authors.

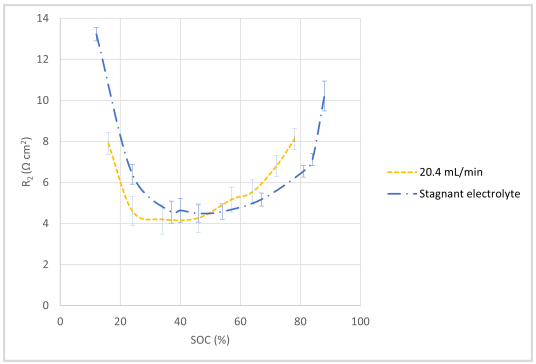

Figure 10: Evolution of R_2 with SOC with and without electrolyte circulation.

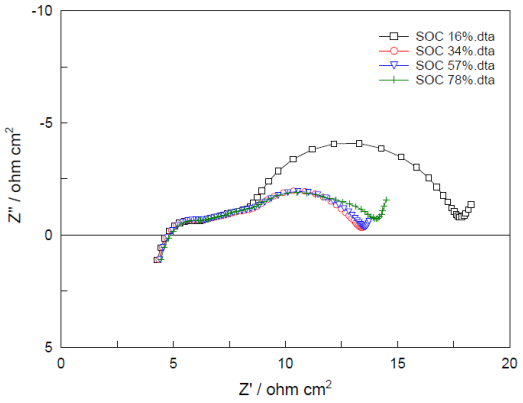

Figure 8: Impedance spectra of the VRFC obtained for different levels of SOC; vanadium concentration of 0.125 M and flow rate of 20.4 mL/min.

To study the effect of the active surface area on the charge-transfer resistance, impedance was measured when removing the carbon felts of both electrodes for a vanadium concentration of 1.21 M. According to the supplier, 3.5 felts with a mass of 10.2002 g will have an active surface area of 16 m^2. The ratio between the charge-transfer resistance of both experiments, with and without carbon felts, is 15.2, which confirms the inverse proportionality between the cell's impedance and the surface active area. The small deviation is most likely caused by some water leftover present in the carbon felts that increase the weight.

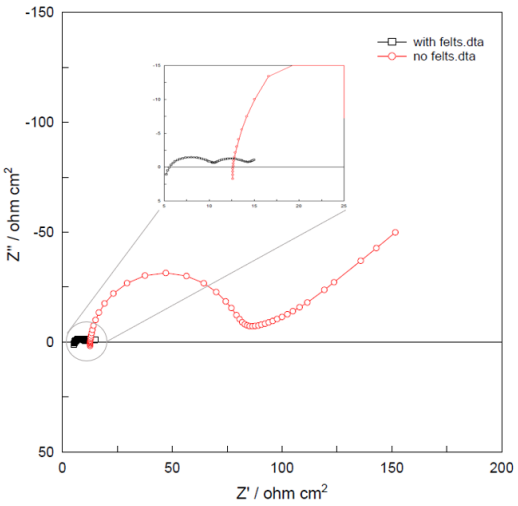

Figure 11: Impedance spectra of the VRFC with and without carbon felts; vanadium concentration of 1.21 M and flow rate of 20.4 mL/min.

6. Economic Evaluation

The economic feasibility of installing a VRFB system in a commercial facility was performed considering the big "Recheio" Supermarket from the company "Jerónimo Martins", in Tavira, Portugal. Assumptions of a daily charge demand of 360 kW and the existence of a PV system with peak production of 556 kWp were made. A 1 MWh/250 kW nominal power battery was considered. An investment cost of 389 500 € was predicted, and annual costs of operation and maintenance of 27 625 €. The energy savings everyday in winter and energy can be taken from Figures 12 and 13, and consequent money savings in the electricity bill were therefore computed.

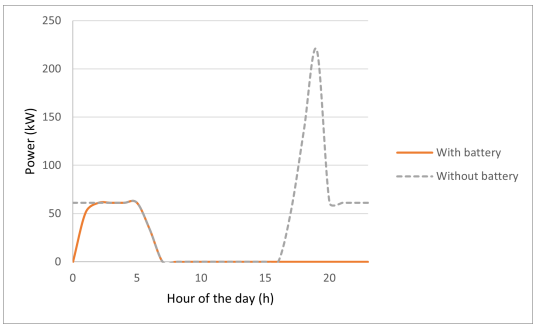

Figure 12: Power demanded to the grid during summer when a VRFB is and is not installed.

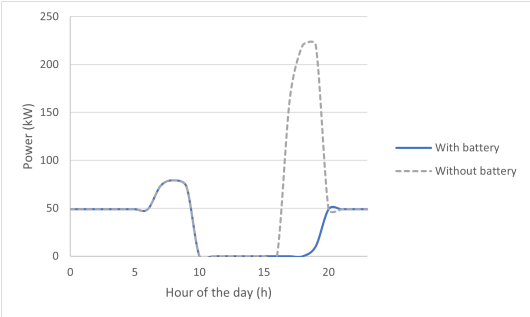

Figure 13: Power demanded to the grid during the winter when a VRFB is and is not installed.

Table 1: Economic parameters calculated for each BESS technology.

	VRFB	Li-ion	Lead-acid
NPV (€)	43 247	-206 258	-95 645
ROI (%)	7.5	8.4	9.8
IRR (%)	4.2	-3.5	-0.45

From Table 1 it is clear that the VRFB installation is the only project that will be economically profitable after 20 years. The other technologies present negative values of NPV and IRR because because they need to be replaced after 10 years. The extended life-time of VRFB is therefore the key factor for the competitiveness of this technology, compensating for relatively low round-trip efficiency and high investment costs.

7. Discussion

In the characterization of the VRFC, assembling of the cell proved to be a sensitive factor, as leaking of highly acidic electrolyte needs to be carefully avoided with precise tightening of the screws.

The formal potential computed of 1.43 V depends greatly on the composition of electrolyte, which can explain the deviations seen from values obtained by other authors, 1.4 V [17, 10] and 1.35 V [7]. Differences in viscosity for different SOC and in kinetics of the reactions make the symmetry of the charge/discharge curves assumed for the determination of the formal potential to deviate from reality.

Good coulombic efficiency above 96% was achieved during charge/discharge processes in the cell, in agreement with results obtained by Wang et al [21]. However, charge/discharge curves while circulating the electrolyte were inconclusive: a cut-off voltage of 1.8 V was imposed, in order to prevent overcharging, but was achieved inside the cell before the electrolyte in the tanks was fully charged, specially for currents above 4 mA/cm^2, possibly due to mass transport issues in the felts. For higher cur-

rents, charging in steps was an option, and current densities were frequently below the current values claimed in the literature, of 25 to 100 mA/cm^2 [7, 8].

Valid conclusions were taken from EIS results despite some difficulties felt at reaching reproducibility of results. The ohmic resistance of the membrane was found to be 97% of the total ohmic resistance of the cell, which shows that improvements in this component will have high impact in the cell's performance. A slight increase in the ohmic resistance for a more concentrated electrolyte can be explained by increased viscosity of the solution.

When studying the effect of the SOC in the impedance spectra, only one arc one arc was observed instead of two. When only one arc is observed, contribution of both charge-transfer and mass transport effects can be reflected on the singular semi-circle [9].

Mass transport effects were reflected differently when removing the carbon felts. The semi-infinite linear behavior is explained by the absence of carbon felts, which enhances the diffusional effects in transport of mass.

The economic evaluation of VRFB applied to a commercial facility in Tavira presented this technology as very competitive in comparison with other technologies. Some authors present different perspectives, including the total disbelief in the economic attractiveness of electrochemical batteries in general due to high investment costs [18, 13, 5]. Regardless of divergence, which is also enhanced by different parameters used in calculation like the batteries' efficiency, depth of discharge and investment costs, the extended life-time of VRFB stand out as a major advantage and even if the total value of the project after 20 years is not so high, the environmental benefits of resorting to more solar energy are key factors supporting the utilization of such technology.

8. Conclusions

Electrochemical Impedance Spectroscopy was successful in studying the electrochemical behavior of the cell without disrupting the properties of the system. The ohmic resistance computed for a vanadium concentration of 0.125 M was 3.9 Ω cm^2, the Nafion 117 membrane resistance being 3.8 Ω cm^2. The charge-transfer resistance ranged from 3.8 to 13 Ω cm^2, its lower value at 30-70% SOC. Finite transport and semi-infinite linear transport were observed at low frequencies with and without carbon felts, respectively.

Economic assessment for the installation of a VRFB system at the "Recheio" Supermarket in Tavira reached profitability after a 20 year timespan, unlike li-ion and lead-acid, mostly due to their extended life-time.

9. Perspectives for Future Work

Future work around this topic should include further EIS testing using a set-up of two cells in series to control OCP in real-time, preferably at high vanadium concentration. Cell's performance could be improved with different geometries and flow rates, and new methods of membrane activation could possibly decrease its resistance, increasing the cell's performance.

References

[1] Characterisation of batteries by electrochemical impedance spectroscopy. *Energy Reports*, 6:232–241, 2020.

[2] D. Aaron, Z. Tang, A. B. Papandrew, and T. A. Zawodzinski. Polarization curve analysis of all-vanadium redox flow batteries. *Journal of Applied Electrochemistry*, 41(10):1175–1182, 2011.

[3] T. Chen, Y. Jin, H. Lv, A. Yang, M. Liu, B. Chen, Y. Xie, and Q. Chen. Applications of Lithium-Ion Batteries in Grid-Scale Energy Storage Systems. *Transactions of Tianjin University*, 26(3):208–217, 2020.

[4] A. R. Dehghani-Sanij, E. Tharumalingam, M. B. Dusseault, and R. Fraser. Study of energy storage systems and environmental challenges of batteries. *Renewable and Sustainable Energy Reviews*, 104(November 2018):192–208, 2019.

[5] M. Fisher, J. Apt, and J. F. Whitacre. Can flow batteries scale in the behind-the-meter commercial and industrial market? A techno-economic comparison of storage technologies in California. *Journal of Power Sources*, 420(March):1–8, 2019.

[6] Y. A. Gandomi, D. S. Aaron, J. R. Houser, M. C. Daugherty, J. T. Clement, A. M. Pezeshki, T. Y. Ertugrul, D. P. Moseley, and M. M. Mench. Critical Review—Experimental Diagnostics and Material Characterization Techniques Used on Redox Flow Batteries. *Journal of The Electrochemical Society*, 165(5):A970–A1010, 2018.

[7] T. Haisch, H. Ji, and C. Weidlich. Monitoring the state of charge of all-vanadium redox flow batteries to identify crossover of electrolyte. *Electrochimica Acta*, 336, 2020.

[8] S. Kim, J. Yan, B. Schwenzer, J. Zhang, L. Li, J. Liu, Z. Yang, and M. A. Hickner. Cycling performance and efficiency of sulfonated poly(sulfone) membranes in vanadium redox flow batteries. *Electrochemistry Communications*, 12(11):1650–1653, 2010.

[9] P. Leuaa, D. Priyadarshani, D. Choudhury, R. Maurya, and M. Neergat. Resolving charge-transfer and mass-transfer processes of VO2+/VO2+ redox species across the electrode/electrolyte interface using electrochemical impedance spectroscopy for vanadium redox flow battery. *RSC Adv.*, 10(51):30887–30895, 2020.

[10] Y. Li, J. Bao, M. Skyllas-Kazacos, M. P. Akter, X. Zhang, and J. Fletcher. Studies on dynamic responses and impedance of the vanadium redox flow battery. *Applied Energy*, 237(June 2018):91–102, 2019.

[11] Z. Liu and Y. Zou. Vanadium Flow Batteries: Principles, Chracteristics, Structure, Evaluation. In J. Z. Huamin Zang, Xianfeng Li, editor, *Redox Flow Batteries: Fundamentals and Applications*, chapter 3, pages 77–126. CRC Press, Boca Raton, 2018.

[12] E. Lockhart, X. Li, S. Booth, J. Salasovich, D. Olis, J. Elsworth, and L. Lisell. Comparative Study of Techno-economics of Lithium-ion and Lead-acid Batteries in Micro-grids in Sub-Saharan Africa. Technical report, National Renewable Energy Laboratory, 2019.

[13] G. Lorenzi, R. da Silva Vieira, C. A. Santos Silva, and A. Martin. Techno-economic analysis of utility-scale energy storage in island settings. *Journal of Energy Storage*, 21(January 2019):691–705, 2019.

[14] G. J. May, A. Davidson, and B. Monahov. Lead batteries for utility energy storage: A review. *Journal of Energy Storage*, 15:145–157, 2018.

[15] S. Pujiastuti and H. Onggo. Effect of various concentration of sulfuric acid for Nafion membrane activation on the performance of fuel cell. *AIP Conference Proceedings*, 1711(February 2016), 2016.

[16] D. V. Ribeiro, C. A. C. Souza, and J. C. C. Abrantes. Use of Electrochemical Impedance Spectroscopy (EIS) to monitoring the corrosion of reinforced concrete. *Revista IBRACON de Estruturas e Materiais*, 8:529–546, 2015.

[17] A. Tang, J. Bao, and M. Skyllas-Kazacos. Dynamic modelling of the effects of ion diffusion and side reactions on the capacity loss for vanadium redox flow battery. *Journal of Power Sources*, 196(24):10737–10747, 2011.

[18] E. Telaretti, G. Graditi, M. G. Ippolito, and G. Zizzo. Economic feasibility of stationary electrochemical storages for electric bill management applications: The Italian scenario. *Energy Policy*, 94:126–137, 2016.

[19] L. V. Thomas, O. Schmidt, A. Gambhir, S. Few, and I. Staffell. Comparative life cycle assessment of lithium-ion battery chemistries for residential storage. *Journal of Energy Storage*, 28(September 2019):101230, 2020.

[20] C. A. Vincent and B. Scrosati. *Modern Batteries*. Butterworth-Heinemann, Linacre House, Jordan Hill, Oxford OX2 8DP, 2nd edition, 1997.

[21] T. Wang, S. J. Moon, D.-S. Hwang, H. Park, J. Lee, S. Kim, Y. M. Lee, and S. Kim. Selective ion transport for a vanadium redox flow battery (VRFB) in nano-crack regulated proton exchange membranes. *Journal of Membrane Science*, 583:16–22, 2019.